STRUCTURAL CHEMISTRY

ISSN 2053-2296

8-Furylimidazolo-2′-deoxycytidine: crystal structure, packing, atropisomerism and fluorescence

Simone Budow-Busse,[a] Sunit K. Jana,[a] Dasharath Kondhare,[a] Constantin Daniliuc[b] and Frank Seela[a,c]*

[a]Laboratory of Bioorganic Chemistry and Chemical Biology, Center for Nanotechnology, Heisenbergstrasse 11, 48149 Münster, Germany, [b]Organisch-Chemisches Institut, Westfälische Wilhelms-Universität Münster, Corrensstrasse 40, 48149 Münster, Germany, and [c]Laboratorium für Organische und Bioorganische Chemie, Institut für Chemie, Universität Osnabrück, Barbarastrasse 7, 49069 Osnabrück, Germany. *Correspondence e-mail: frank.seela@uni-osnabrueck.de

Received 18 August 2021
Accepted 28 January 2022

Edited by E. Y. Cheung, Moderna Inc., USA

Keywords: 8-furylimidazolo-2′-deoxycytidine; crystal structure; atropisomerism; crystal packing; Hirshfeld surface analysis; fluorescence.

CCDC reference: 2095197

Supporting information: this article has supporting information at journals.iucr.org/c

8-Furylimidazolo-2′-deoxycytidine (^{fur}ImidC), $C_{14}H_{14}N_4O_5$, is a fluorescent analogue of 2′-deoxycytidine, also displaying the same recognition face. As a constituent of DNA, ^{fur}ImidC forms extraordinarily strong silver-mediated self-pairs. Crystal structure determination revealed that ^{fur}ImidC adopts two types of disordered residues: the sugar unit and the furyl moiety. The disorder of the sugar residue amounts to an 87:13 split. The disorder of the furyl ring results from axial chirality at the C8—C2″ bond connecting the nucleobase to the heterocycle. The two atropisomers are present in unequal proportions [occupancies of 0.69 (2) and 0.31 (2)], and the nucleobase and the furyl moiety are coplanar. Considering the atomic sites with predominant occupancy, an *anti* conformation with $\chi = -147.2\ (7)^\circ$ was found at the glycosylic bond and the 2′-deoxyribosyl moiety shows a C2′-*endo* (S, $^2T_1$) conformation, with $P = 160.0^\circ$. A ^{1}H NMR-based conformational analysis of the furanose puckering revealed that the *S* conformation predominates also in solution. In the solid state, two neighbouring ^{fur}ImidC molecules are arranged in a head-to-tail fashion, but with a notable tilt of the molecules with respect to each other. Consequently, one N—H···N hydrogen bond is found for neighbouring molecules within one layer, while a second N—H···N hydrogen bond is formed to a molecule of an adjacent layer. In addition, hydrogen bonding is observed between the nucleobase and the sugar residue. A Hirshfeld surface analysis was performed to visualize the intermolecular interactions observed in the X-ray study. In addition, the fluorescence spectra of ^{fur}ImidC were measured in solvents of different polarity and viscosity. ^{fur}ImidC responds to microenvironmental changes (polarity and viscosity), which is explained by a hindered rotation of the furyl residue in solvents of high viscosity.

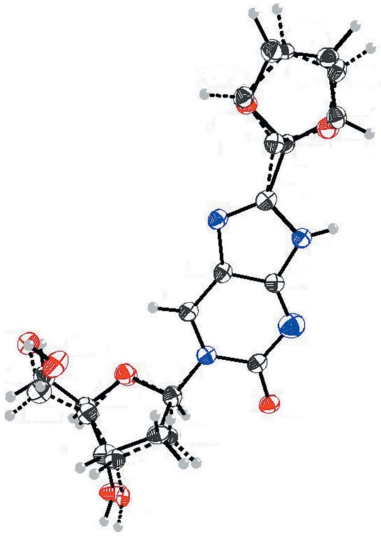

1. Introduction

8-Furylimidazolo-2′-deoxycytidine (^{fur}ImidC, **1**) is a base-modified nucleoside with the recognition face of 2′-deoxycytidine (dC, **5**) (Jana *et al.*, 2015) (purine numbering is used throughout this article). This nucleoside displays a strong fluorescence as it is composed of the fluorescent nucleobase 2-hydroxypurine carrying a furyl system at the 8-position and a sugar moiety linked to the N atom at the 1-position (Fig. 1). The related nucleoside 2′-deoxyisoinosine (**3**), with the sugar moiety linked to the 9-position, is also fluorescent (Seela *et al.*, 1994, 2000; Seela & Chen, 1995). As a constituent of DNA, ^{fur}ImidC (**1**) shows unique properties, as it forms strong base pairs with dG and extremely strong silver-mediated self-pairs (Jana *et al.*, 2015).

Imidazolo-2′-deoxycytidine (**2**) is structurally related to pyrrolo-2′-deoxycytidine (pyrrolo-dC, **4**), a fluorescent dC congener with a pyrrolo[2,3-*d*]pyrimidine instead of the purine

Table 1
Experimental details.

Crystal data	
Chemical formula	$C_{14}H_{14}N_4O_5$
M_r	318.29
Crystal system, space group	Orthorhombic, $P2_12_12_1$
Temperature (K)	100
a, b, c (Å)	5.3043 (4), 11.1405 (8), 22.6067 (18)
V (Å^3)	1335.89 (18)
Z	4
Radiation type	Cu $K\alpha$
μ (mm^{-1})	1.04
Crystal size (mm)	0.38 × 0.06 × 0.03
Data collection	
Diffractometer	Bruker D8 Venture PHOTON 100 CMOS
Absorption correction	Multi-scan (*SADABS*; Bruker, 2014)
T_{min}, T_{max}	0.69, 0.97
No. of measured, independent and observed [$I > 2\sigma(I)$] reflections	28381, 2241, 1559
R_{int}	0.149
(sin $\theta/\lambda)_{max}$ (Å^{-1})	0.588
Refinement	
$R[F^2 > 2\sigma(F^2)]$, $wR(F^2)$, S	0.053, 0.142, 1.03
No. of reflections	2241
No. of parameters	335
No. of restraints	279
H-atom treatment	H atoms treated by a mixture of independent and constrained refinement
$\Delta\rho_{max}$, $\Delta\rho_{min}$ (e Å^{-3})	0.22, −0.20
Absolute structure	Flack x determined using 503 quotients $[(I^+) - (I^-)]/[(I^+) + (I^-)]$ (Parsons *et al.*, 2013)
Absolute structure parameter	0.0 (3)

Computer programs: *APEX3* (Bruker, 2016), *SAINT* (Bruker, 2015), *SHELXT2014* (Sheldrick, 2015*a*), *SHELXL2018* (Sheldrick, 2015*b*), *shelXle* (Hübschle *et al.*, 2011) and *SHELXL2014* (Sheldrick, 2015*b*).

skeleton of **2**. Pyrrolo-dC (**4**) (Inoue *et al.*, 1987) has been incorporated into DNA and base pairs selectively with dG without disturbing the Watson–Crick duplex structure (Hudson & Ghorbani-Choghamarani, 2007; Wilhelmsson, 2010).

While much work has been performed on pyrrolo-dC and its derivatives (Tinsley & Walter, 2006; Wahba *et al.*, 2010; Ming & Seela, 2012; Noé *et al.*, 2012), reports of studies on ImidC (**2**) are rare. Fischer and co-workers synthesized a series of *para*-substituted imidazolocytidines and incorporated 8-(*p*-CF_3-phenyl)imidazolo-2′-deoxycytidine into oligonucleotides to study mismatch discrimination (Kovaliov *et al.*, 2013, 2014). Recently, it was shown that substituted imidazolo-2′-deoxycytidines can function as effective silver-ion binders (Mei *et al.*, 2014). In DNA, self-pairs of imidazolo-2′-deoxycytidines form silver-mediated base pairs in which silver ions take over the function of protons in semiprotonated 'dC–dC' base pairs (Mei *et al.*, 2014; Clever *et al.*, 2007). In this context, 8-furylimidazolo-2′-deoxycytidine (^{fur}ImidC, **1**), decorated with a furyl substituent at the 8-position (Fig. 1), was designed (Jana *et al.*, 2015). The furyl moiety is anticipated to enhance the coordination forces for silver ions to the system. Also, the fluorescence properties of **1** are improved compared to the unmodified ImidC (**2**).

In addition, the ^{fur}ImidC (**1**) molecule comprises a distinctive feature, namely, the presence of the furyl substituent, which enables the molecule to form atropisomers. Atropisomerism is a dynamic type of axial chirality with stereochemically hindered rotation about single bonds and can generate a mixture of two isomers.

To verify the formation of atropisomers, an X-ray analysis of 8-furylimidazolo-2′-deoxycytidine (**1**) was performed. The conformation of ^{fur}ImidC (**1**) in the solid state and in solution, as well as the crystal packing of the molecule, were studied. Solvent-dependent fluorescence spectra of **1** were determined to monitor the impact of microenvironmental changes in solution.

2. Experimental

2.1. Synthesis and crystallization of ^{fur}ImidC (1)

8-Furylimidazolo-dC (**1**) was synthesized as reported by Jana *et al.* (2015). For crystallization, compound **1** was dissolved in water and was obtained as colourless needles by slow evaporation of the solvent at room temperature. A needle-like specimen of **1** was used for the X-ray crystallographic analysis.

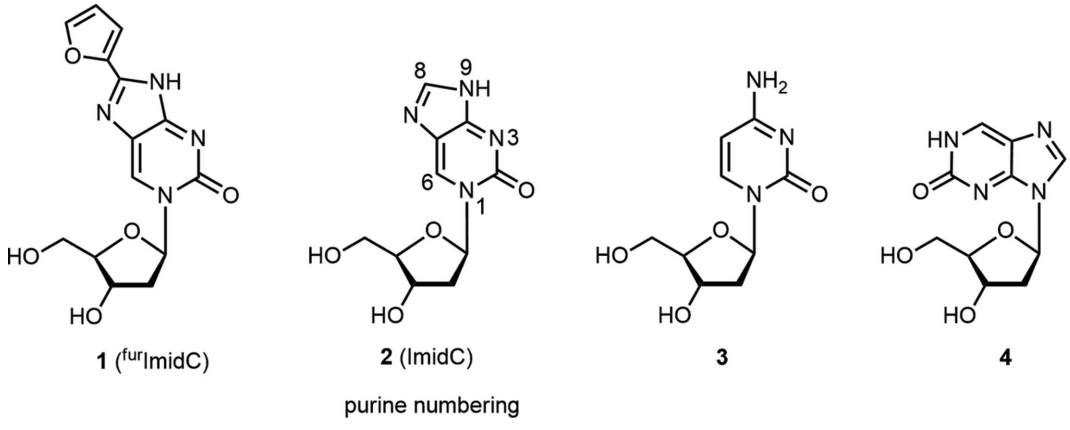

Figure 1
Imidazolo-dC nucleosides and close derivatives.

2.2. Refinement

Crystal data, data collection and structure refinement details are summarized in Table 1. The H atom at the N9 atom was refined freely. Moreover, the furyl ring and the sugar moiety linked to atom N1 are disordered over two positions. Several restraints (*SHELXL* instructions SADI, SAME, ISOR and SIMU) were used in order to improve refinement stability. Full details of the refinement instructions can be found embedded in the CIF.

3. Results and discussion

3.1. Molecular geometry and conformation of 8-furyl-imidazolo-dC (1)

The crystals of ^{fur}ImidC (**1**) are orthorhombic with the space group $P2_12_12_1$. For selected geometric parameters, see Table 2. The three-dimensional (3D) structure of ^{fur}ImidC (**1**) is shown in Fig. 2 and shows two sets of disordered groups. The furyl group is rotationally disordered over two positions having occupancies of 0.69 (2) (solid line) and 0.31 (2) (dashed line). The second disorder concerns the sugar residue, but it is less pronounced, with occupancies of 0.86 (7) and 0.13 (3).

The disordered sites of the furyl ring are related to each other by a rotation of 180° about the C8—C2″ bond (Fig. 3). Accordingly, the two isomers are atropisomers (Clayden *et al.*, 2009; Toenjes & Gustafson, 2018) and the C8—C2″ bond is a chiral axis. Considering the composition of the entire ^{fur}ImidC (**1**) molecule including the attached sugar residue, the isomers are diastereomeric comprising different physical properties. This might also contribute to the unequal proportion of both atropisomers within the crystal. Most interestingly, different to

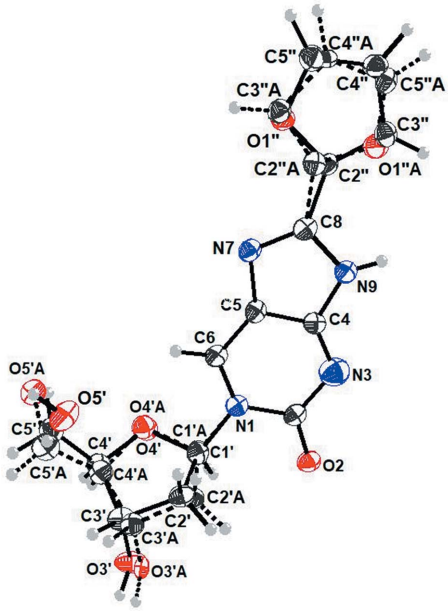

Figure 2
Perspective view of 8-furylimidazolo-dC (**1**), showing the atomic numbering scheme. The major disorder component has been drawn using full lines and the minor disorder component has been drawn using dashed lines. Displacement ellipsoids are drawn at the 50% probability level and H atoms are shown as small spheres of arbitrary size.

Table 2
Selected geometric parameters (Å, °).

O2—C2	1.244 (6)	N1—C1′*A*	1.47 (3)
C8—C2″*A*	1.418 (19)	N1—C1′	1.477 (8)
C8—C2″	1.451 (11)		
N7—C8—C2″*A*	116.1 (14)	C2—N1—C1′*A*	117 (2)
N9—C8—C2″*A*	130.4 (14)	C2—N1—C1′	117.4 (6)
N7—C8—C2″	128.2 (8)	O5′—C5′—C4′	110.8 (8)
N9—C8—C2″	118.3 (8)	O5′*A*—C5′*A*—C4′*A*	114 (4)
N9—C8—C2″—O1″	177.7 (12)	C3′—C4′—C5′—O5′	47.3 (10)
N9—C8—C2″*A*—O1″*A*	1 (5)	C2—N1—C1′*A*—O4′*A*	−162 (3)
C2—N1—C1′—O4′	−147.2 (7)	C3′*A*—C4′*A*—C5′*A*—O5′*A*	164 (6)

other nucleosidic compounds forming atropisomers, *e.g.* pyrrolopyrimidine-based (PPY) kinase inhibitors (Smith *et al.*, 2015), the nucleobase and the furyl ring of ^{fur}ImidC (**1**) are coplanar in both atropisomers. The crystal structure of a PPY inhibitor showed a perpendicular arrangement of the nucleobase and the attached benzyl ring (Smith *et al.*, 2015). This difference can probably be attributed to the fact that the furyl ring of ^{fur}ImidC (**1**) does not carry any bulky substituents. This lowers the energy barrier for atropisomer interconvertion of ^{fur}ImidC (**1**) to such an extent that both isomers become inseparable in solution at room temperature.

As the nucleobase shows no disorder and the sugar residue adopts only a minor disorder, the conformational analysis of ^{fur}ImidC (**1**) was carried out mainly considering the atomic sites with predominant occupancy. The torsion angle χ (O4′—C1′—N1—C2) (IUPAC–IUB Joint Commission on Biochemical Nomenclature, 1983) of ^{fur}ImidC (**1**) is defined in analogy to pyrimidine nucleosides, as this molecule can be considered a pyrimidine nucleoside analogue with a fused imidazole ring and a furyl substituent. The orientation of the nucleobase with oxygen-2 of the pyrimidine ring pointing away from the sugar moiety refers to an *anti* conformation (Saenger, 1984). The *syn* conformation is adopted when oxygen-2 is pointing towards the sugar ring. Natural pyrimidine 2′-deoxyribonucleosides, including 2′-deoxycytidine (**5**), prefer an *anti* conformation (Young & Wilson, 1975). Also for ^{fur}ImidC (**1**), an *anti* conformation is found around the glycosylic bond, with χ = −147.2 (7)°.

Moreover, the 8-furyl substituent of **1** is connected to the imidazole residue *via* an aryl–aryl bond and is coplanar with the nucleobase. In the solid state, the C8—C2″ bond becomes

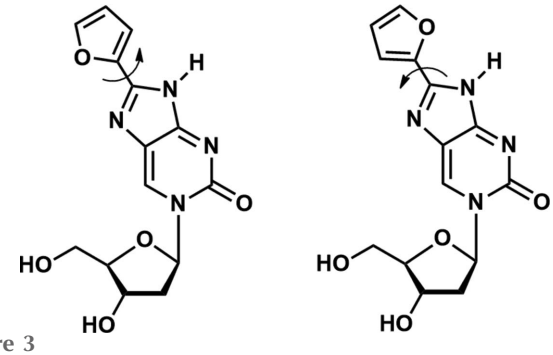

Figure 3
Atropisomerism of 8-furylimidazolo-2′-deoxycytidine (**1**).

a chiral axis due to atropisomerism. The bond length is 1.451 (11) Å for the major atropisomer and somewhat shorter for the minor atropisomer [C8—C2″*A* = 1.418 (19) Å] (Table 2). The length of the glycosylic C1′—N1 bond connecting the nucleobase and sugar is 1.477 (8) Å (Table 2).

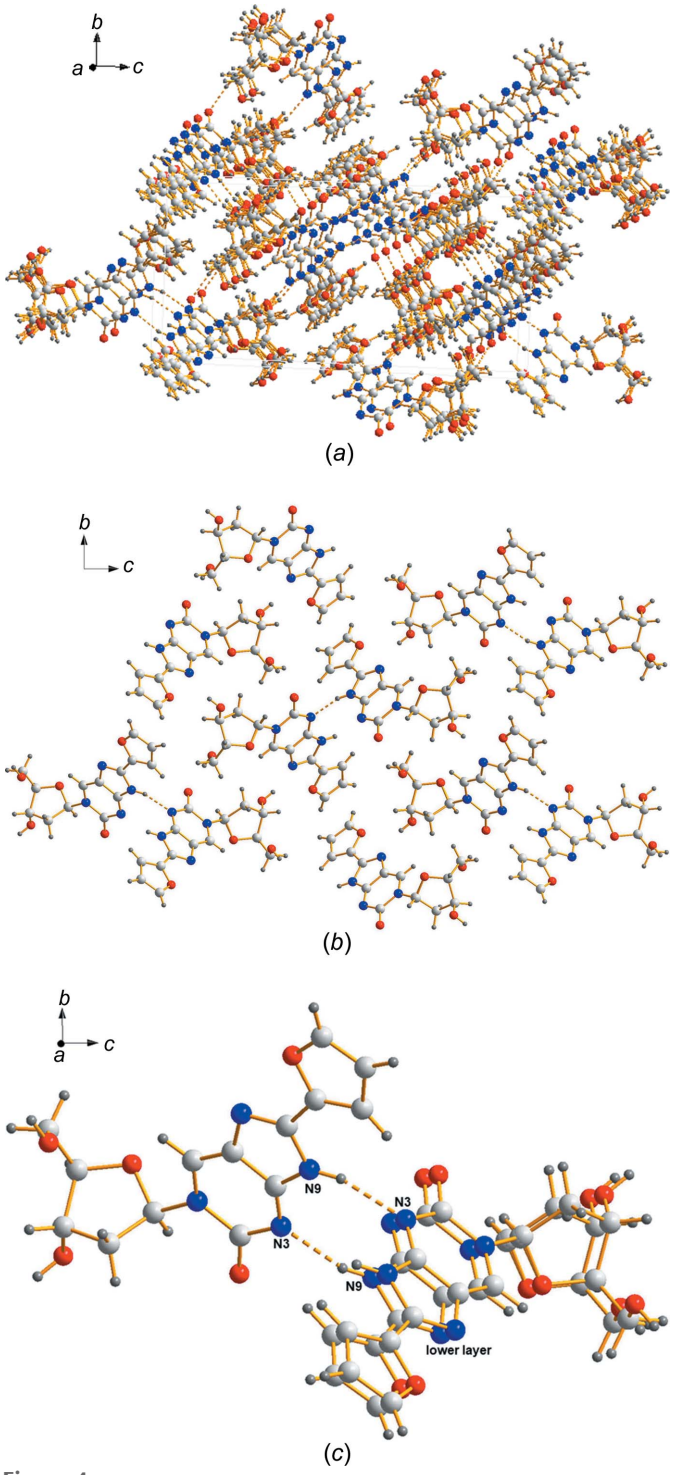

Figure 4
(*a*) Multilayered packing of **1**, showing the stacking interactions of the molecules. (*b*) Hydrogen bonding of ^{fur}ImidC (**1**) within the *bc* plane. (*c*) Self-pairing of ^{fur}ImidC (**1**), with a head-to-tail alignment, and showing the contacts of one molecule to two neighbouring molecules. For clarity, the minor disorder components have been omitted from parts (*b*) and (*c*).

This is in the range of the average length (1.49 Å) of glycosylic bonds observed for pyrimidine nucleosides (Saenger, 1984).

The orientation of the exocyclic 5′-hydroxy group relative to the sugar ring is characterized by the torsion angle γ (O5′—C5′—C4′—C3′) (Saenger, 1984). For ^{fur}ImidC (**1**), a synclinal (+*sc*) conformation with γ = 47.3 (10)° is observed, which is the preferred conformation in pyrimidine nucleosides (Saenger, 1984).

The sugar pucker of the 2′-deoxyribofuanosyl moiety is another major parameter for characterizing the conformation of nucleosides. In correlation to the major displacement of C3′ or C2′ from the median plane of C1′—O4′—C4′, nucleosides can adopt two principal sugar puckering modes, namely, C3′-*endo* (*N*) and C2′-*endo* (*S*) (Altona & Sundaralingam, 1972; Saenger, 1984). The C2′-*endo* conformation is the preferred puckering mode of canonical 2′-deoxyribonucleosides. Also, the sugar moiety of ^{fur}ImidC (**1**) adopts C2′-*endo* (*S*, $^{2}T_{1}$) conformation with a pseudorotational phase angle *P* = 160.0° and a maximum amplitude τ_m = 35.6° (Altona & Sundaralingam, 1972; Saenger, 1984).

However, the solid-state conformation of nucleosides is not necessarily identical to the nucleoside conformation observed in solution or as constituents of DNA. The population of *S versus N* conformers is rapidly interconverting in solution and shows a preference for one conformation (Saenger, 1984). In this regard and to confirm the sugar conformation of ^{fur}ImidC (**1**) in solution, a conformational analysis of the furanose puckering of ^{fur}ImidC (**1**) was performed. For this, a high-resolution ^{1}H NMR spectrum of compound **1** was measured in dimethyl sulfoxide (DMSO) and coupling constants were determined. The ^{1}H NMR spectrum (Fig. S4) and the coupling constants (Table S2) are available in the supporting information. The program *PSEUROT* (Version 6.3; Van Wijk *et al.*, 1999) was used to carry out the conformational analysis of the sugar puckering of the 2′-deoxyribofuranosyl ring. This program calculates the population of the *N*- and *S*-type conformers on the basis of five ^{3}J(H,H) coupling constants, namely, ^{3}J(H1′,H2′), ^{3}J(H1′,H2"), ^{3}J(H2′,H3′), ^{3}J(H2″,H3′) and ^{3}J(H3′,H4′). The *PSEUROT* analysis of ^{fur}ImidC (**1**) showed that the 2′-deoxyribofuranosyl moiety of this nucleoside prefers the *S* conformation (57%) in solution. However, compared to the canonical 2′-deoxycytidine (**5**) (72% *S*), the *S* population of **1** is less pronounced (Budow-Busse *et al.*, 2021).

Taken together, despite the fact that compound **1** carries a nucleobase consisting of a pyrimidine moiety with a fused imidazole ring (corresponding to N1-glycosylated 2-hydroxypurine), this nucleoside adopts conformational properties typical for pyrimidine 2′-deoxyribonucleosides.

3.2. Hydrogen bonding and molecular packing of ^{fur}ImidC (1)

Within the extended network, the molecules of ^{fur}ImidC (**1**) are stacked on each other, forming piles of nucleobases and sugar residues as shown in Fig. 4(*a*). Details of the arrangement of the individual molecules are highlighted in Figs. 4(*b*) and 4(*c*). As 8-furylimidazolo-dC (**1**) shows strong self-pairing properties within the DNA double helix (Jana *et al.*, 2015),

with a head-to-head alignment of the nucleobases in anti-parallel-stranded (aps) DNA and a head-to-tail arrangement in parallel-stranded (ps) DNA, we assumed that one of these two pairing motifs will be observed in the solid-state structure of ^{fur}ImidC (**1**). In fact, we found a kind of head-to-tail arrangement of two neighbouring nucleoside molecules, but with a notable tilt of the molecules with respect to each other. As a consequence, instead of two expected N—H···N hydrogen bonds with N9 of the imidazole ring of one molecule as hydrogen-bond donor and N3 of the pyrimidine ring of another molecule as acceptor, only one of these contacts is found for neighbouring molecules (N9—H9···N3^{i}; for hydrogen-bonding data and symmetry codes, see Table 3). Due to the tilted arrangement of the molecules, the second possible N9—H9···N3^{i} contact is observed to a ^{fur}ImidC (**1**) molecule of another layer [Fig. 4(*c*)]. In addition, hydrogen bonding is observed between the nucleobase, with N7 and O2 as acceptors and O3′ (O3′*A*—H3′1*A*···N7^{ii}) as well as O5′ (O5′*A*—H5′*A*···O2^{iii}) of the sugar residue as hydrogen-bond donors [Fig. 4(*a*)]. The furyl substituent does not participate in hydrogen bonding.

3.3. Hirshfeld surface analysis of ^{fur}ImidC (1)

Hirshfeld surface analysis, including 3D surfaces and two-dimensional (2D) fingerprint plots, represent a convenient method for obtaining and visualizing information on intermolecular interactions (Spackman & Jayatilaka, 2009). The program *CrystalExplorer* (Version 17; Spackman & Jayatilaka, 2009; Turner *et al.*, 2017) was used to conduct the Hirshfeld surface analysis of 8-furylimidazolo-dC (**1**) mapped with a d_{norm} range of −0.5 to 1.5 Å, shape index (−1.0 to 1.0 Å; Fig. S1 in the supporting information) and curvedness (−4.0 to 0.4 Å), as well as the corresponding 2D fingerprint plots. The individual hydrogen-bonding interactions were identified on the d_{norm} surfaces as large circular areas (intense red spots). These red areas indicate the close N—H···N, O—H···N and O—H···O contacts, as these interactions are shorter than the sum of the van der Waals radii and show negative d_{norm} [Fig. 5(*a*)]. The results of the Hirshfeld analyses are consistent with the hydrogen-bonding data (Table 3). Moreover, the large flat region across the nucleobase of ^{fur}ImidC (**1**) visible on the curvedness surface plots indicates π–π interactions [Fig. 5(*b*)]. This observation fits the pronounced stacking interactions of molecule **1**, as indicated in Fig. 4(*a*). Fig. 5(*c*) shows the overall 2D fingerprint plot of 8-furylimidazolo-dC (**1**) and those resolved into O···H/H···O, N···H/H···N, C···H/H···C and H···H contacts [Figs. 5(*d*)–(*g*)], together with their relative contributions to the Hirshfeld surface. The proportions of O···H/H···O, N···H/H···N and C···H/H···C interactions comprise 21.7, 12.7 and 9.2%, respectively, of the total Hirshfeld surfaces.

Table 3
Hydrogen-bond geometry (Å, °).

D—H···*A*	*D*—H	H···*A*	*D*···*A*	*D*—H···*A*
N9—H9···N3^{i}	0.87 (3)	2.01 (3)	2.863 (7)	165 (6)
O3′*A*—H3′1*A*···N7^{ii}	0.84	2.08	2.852 (16)	153
O5′*A*—H5′*A*···O2^{iii}	0.84	1.99	2.818 (6)	169

Symmetry codes: (i) $x+\frac{1}{2}, -y+\frac{3}{2}, -z+1$; (ii) $-x, y+\frac{1}{2}, -z+\frac{1}{2}$; (iii) $-x, y-\frac{1}{2}, -z+\frac{1}{2}$.

3.4. ^{fur}ImidC solvent-dependent fluorescence

The nucleobases of the purine or pyrimidine nucleosides are virtually nonfluorescent. They become fluorescent when a

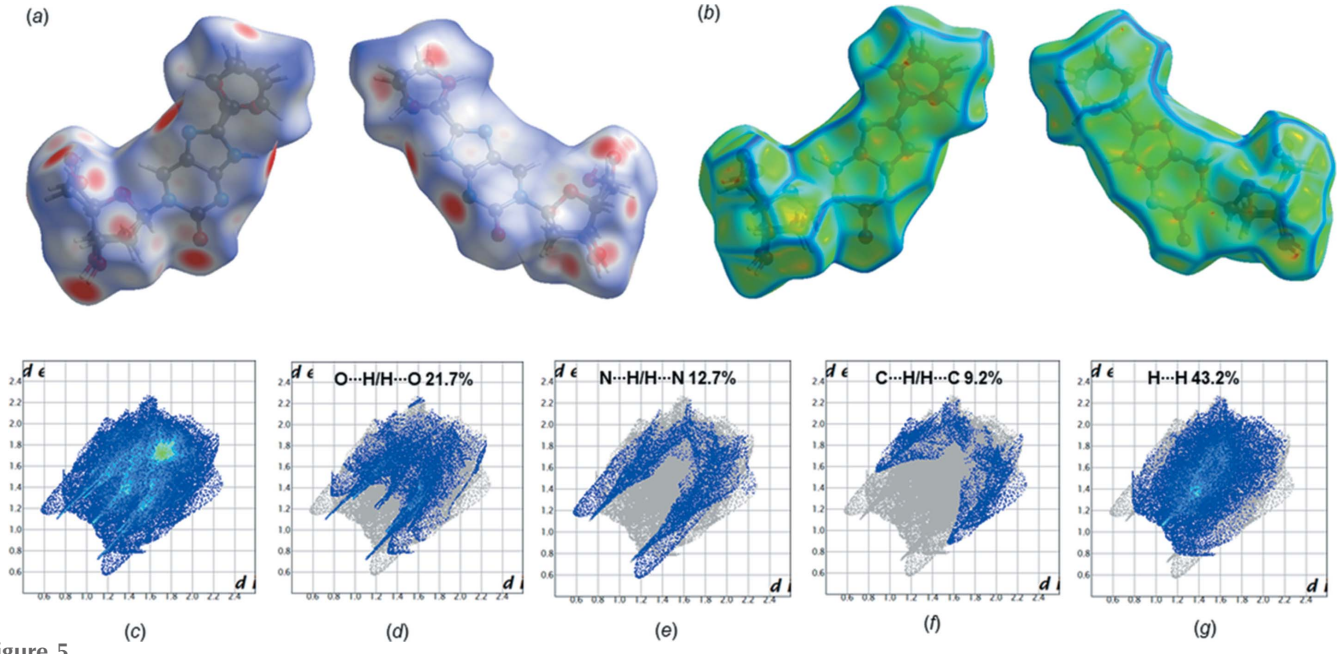

Figure 5
(*a*) Hirshfeld surface of ^{fur}ImidC (**1**) mapped with d_{norm} (−0.5 to 1.5 Å), shown in front and back view. (*b*) Curvedness surface plots (front and back view; −4.0 to 0.4 Å). 2D fingerprint plots showing the percentage contributions of various interactions to the total Hirshfeld surface area of compound **1**: (*c*) full interactions and resolved contacts; (*d*) O···H/H···O; (*e*) N···H/H···N; (*f*) C···H/H···C; (*g*) H···H.

furyl moiety is attached (Greco & Tor, 2007; Sinkeldam *et al.*, 2011). On the contrary, the nucleobase of ^{fur}ImidC (**1**) shows already intrinsic fluorescence (Seela *et al.*, 1994, 2000; Seela & Chen, 1995). Earlier, it was reported that a furyl substituent attached to a pyrimidine or purine nucleobase *via* a rotatable aryl–aryl bond represents a molecular rotor (Lee *et al.*, 2018). However, it was not discussed that axial chirality is introduced into these molecules and atropisomers are formed. This information can be drawn from the crystal structure of ^{fur}ImidC (**1**). Similar to the situation in the crystalline state, the rotation becomes hindered in solvents of high viscosity and therefore a strong impact on the fluorescence is expected. This prompted us to record the fluorescence emission spectra of ^{fur}ImidC (**1**) in solvents of different polarity and viscosity [Fig. 6(*a*)]. For comparison, the fluorescence spectra of ^{ph}ImidC (**6**) were also recorded [Fig. 6(*b*)]. This molecule carries a less polar phenyl substituent which might show weaker interactions with solvent molecules. For Stokes shifts, quantum yields and brightness, see Table S1 in the supporting information.

Already the UV spectra of **1** shows a solvent dependence of the long wavelength maximum centred around 350 nm (Fig. S2 in the supporting information). In the nonpolar solvents DMSO and dimethylformamide (DMF), the UV maxima are bathochromically shifted by around 10 nm compared to the maxima recorded in the polar solvents glycerol and water. For comparison, the UV spectra determined for ^{ph}ImidC (**6**) show similarities but also differences with respect to **1** (Fig. S2 in the supporting information). Herein the maxima at shorter wavelengths are hypsochromically shifted by around 10 nm.

Much stronger solvent dependencies are observed for the fluorescence spectra. Excitation was carried out at the long wavelength maximum of each solvent (Table S1 in the supporting information). The fluorescence of ^{fur}ImidC (**1**) depends strongly on the particular solvent [Fig. 6(*a*)] and much higher quantum yields are observed in water (Φ = 0.69) compared to all other solvents (Table S1). The fluorescence intensity in aprotic solvents of low polarity (DMSO, DMF, MeCN and dioxane) is lower. For nucleoside **6**, the situation is different. The fluorescence intensity is highest in polar protic solvents [Fig. 6(*b*)]. However, the highest quantum yield for **6** was observed in ethylene glycol (Φ = 0.65; Table S1).

The fluorescence obtained in glycerol [$E_T(30)$ = 57.0 kcal mol^{-1}, η = 1.412 Pa s] and ethylene glycol [$E_T(30)$ = 56.3 kcal mol^{-1}, η = 1.61 × 10^{-2} Pa s] are of particular interest, as both solvents exhibit almost comparable polarity but different viscosity (Reichardt, 1994). Indeed, the fluorescence intensity of ^{fur}ImidC (**1**) responds significantly to the viscosity difference. In glycerol, the fluorescence is the weakest (Φ = 0.22), while it is much higher in ethylene glycol (Φ = 0.46) (Table S1). Most interestingly, ^{fur}ImidC (**1**) shows low fluorescence in the highly viscous solvent glycerol and strong fluorescence in the lowly viscous solvent water. For the phenyl-substituted nucleoside **6**, the effect is much weaker. Accordingly, ^{fur}ImidC (**1**) responds strongly to microenvironmental changes (polarity and viscosity) and is in particular

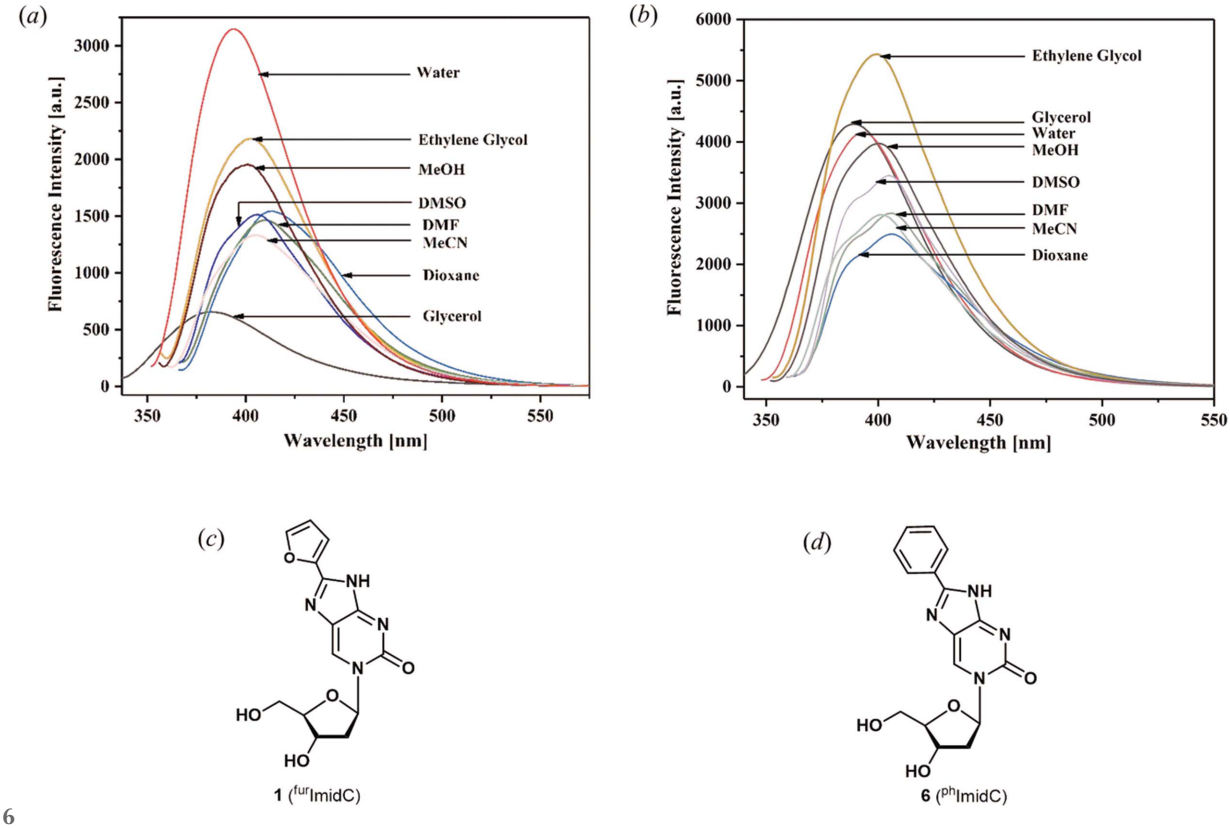

Figure 6
Fluorescence emission spectra measured in solvents of different polarity using a nucleoside concentration of 3 µ*M* and excitation at $\lambda_{abs,max}$ for (*a*) ^{fur}ImidC (**1**) and (*b*) ^{ph}ImidC (**6**). The structures of (*c*) 8-furylimidazolo-dC (^{fur}ImidC, **1**) and (*d*) 8-phenylimidazolo-dC (^{ph}ImidC, **6**).

sensitive against viscosity changes. In fact, it has to be considered that in solution already two atropisomeric molecules are present. This is not only valid for compound **1**, but is a general phenomenon occurring in related purine and pyrimidine nucleosides with unsymmetric heterocycles as side chains, as reported by Tor (Greco & Tor, 2007) and others (Tokugawa *et al.*, 2016).

4. Conclusion

The crystal structure of fluorescent 8-furylimidazolo-2′-deoxycytidine (^{fur}ImidC, **1**) has been studied. In the solid state, ^{fur}ImidC shows two independent types of disordered groups (sugar and furyl moiety). The sugar residue shows a minor disorder (87:13 split), while the disorder of the furyl ring shows a split of ∼30:70. The latter results from atropisomerism at the C8—C2″ chiral axis connecting the nucleobase and the furyl residue. The isomers are related to each other by a 180° rotation, are coplanar and are therefore in conjugation.

For the solid-state conformational analysis of ^{fur}ImidC (**1**), only atoms with the predominant occupancy were used. Nucleoside **1** shows an *anti* conformation at the glycosylic bond [χ = −147.2 (7)°] and a C2′-*endo* (*S*, $^{2}T_{1}$) sugar pucker. In solution, the *S* conformation also predominates, as shown by a ^{1}H NMR-based conformational analysis of the furanose puckering. Stacking interactions of the molecules, as well as hydrogen bonding between two nucleobase moieties and between the nucleobase and the sugar residue, stabilize the crystal structure. Two neighbouring ^{fur}ImidC molecules are arranged in a head-to-tail fashion, but with a notable tilt of the molecules with respect to each other. Consequently, one N9—H9···N3 hydrogen bond is found for neighbouring molecules within one layer, while a second contact with N9 as hydrogen-bond donor and N3 as acceptor is formed to a molecule of an adjacent layer.

The ^{fur}ImidC (**1**) nucleoside shows fluorescence. The fluorescence intensity responds strongly to the viscosity of the solvent due to atropisomerism and the conjugation of the furan system with the imidazolo–pyrimidine heterocycle. This environmental phenomenon might be used to monitor conformational changes in nucleic acids or interactions with proteins.

Acknowledgements

We thank Dr Peter Leonard for critical reading of the manuscript. We would like to thank Professor Dr B. Wünsch, Institut für Pharmazeutische und Medizinische Chemie, Westfälische Wilhelms-Universität Münster, for providing us with the NMR spectra. Funding by ChemBiotech, Münster, Germany, is gratefully acknowledged. Open access funding enabled and organized by Projekt DEAL.

References

Altona, C. & Sundaralingam, M. (1972). *J. Am. Chem. Soc.* **94**, 8205–8212.
Bruker (2014). *SADABS*. Bruker AXS Inc., Madison, Wisconsin, USA.
Bruker (2015). *SAINT*. Bruker AXS Inc., Madison, Wisconsin, USA.
Bruker (2016). *APEX3*. Bruker AXS Inc., Madison, Wisconsin, USA.
Budow-Busse, S., Chai, Y., Müller, S. L., Daniliuc, C. & Seela, F. (2021). *Acta Cryst.* C**77**, 202–208.
Clayden, J., Moran, W. J., Edwards, P. J. & LaPlante, S. R. (2009). *Angew. Chem. Int. Ed.* **48**, 6398–6401.
Clever, G. H., Kaul, C. & Carell, T. (2007). *Angew. Chem. Int. Ed.* **46**, 6226–6236.
Greco, N. J. & Tor, Y. (2007). *Tetrahedron*, **63**, 3515–3527.
Hübschle, C. B., Sheldrick, G. M. & Dittrich, B. (2011). *J. Appl. Cryst.* **44**, 1281–1284.
Hudson, R. H. E. & Ghorbani-Choghamarani, A. (2007). *Synlett*, **6**, 870–873.
Inoue, H., Imura, A. & Ohtsuka, E. (1987). *Nippon Kagaku Kaishi*, pp. 1214–1220.
IUPAC–IUB Joint Commission on Biochemical Nomenclature (1983). *Eur. J. Biochem.* **131**, 9–15.
Jana, S. K., Guo, X., Mei, H. & Seela, F. (2015). *Chem. Commun.* **51**, 17301–17304.
Kovaliov, M., Segal, M. & Fischer, B. (2013). *Tetrahedron*, **69**, 3698–3705.
Kovaliov, M., Weitman, M., Major, D. T. & Fischer, B. (2014). *J. Org. Chem.* **79**, 7051–7062.
Lee, S.-C., Heo, J., Woo, H. C., Lee, J.-A., Seo, Y. H., Lee, C.-L., Kim, S. & Kwon, O.-P. (2018). *Chem. Eur. J.* **24**, 13706–13718.
Mei, H., Ingale, S. A. & Seela, F. (2014). *Chem. Eur. J.* **20**, 16248–16257.
Ming, X. & Seela, F. (2012). *Chem. Eur. J.* **18**, 9590–9600.
Noé, M. S., Ríos, A. C. & Tor, Y. (2012). *Org. Lett.* **14**, 3150–3153.
Parsons, S., Flack, H. D. & Wagner, T. (2013). *Acta Cryst.* B**69**, 249–259.
Reichardt, C. (1994). *Chem. Rev.* **94**, 2319–2358.
Saenger, W. (1984). In *Principles of Nucleic Acid Structure*, edited by C. R. Cantor. New York: Springer-Verlag.
Seela, F., Becher, G. & Chen, Y. (2000). *Nucleosides Nucleotides Nucleic Acids*, **19**, 1581–1598.
Seela, F. & Chen, Y. (1995). *Nucleosides Nucleotides Nucleic Acids*, **14**, 863–866.
Seela, F., Chen, Y., Bindig, U. & Kazimierczuk, Z. (1994). *Helv. Chim. Acta*, **77**, 194–202.
Sheldrick, G. M. (2015*a*). *Acta Cryst.* A**71**, 3–8.
Sheldrick, G. M. (2015*b*). *Acta Cryst.* C**71**, 3–8.
Sinkeldam, R. W., Wheat, A. J., Boyaci, H. & Tor, Y. (2011). *ChemPhysChem*, **12**, 567–570.
Smith, D. E., Marquez, I., Lokensgard, M. E., Rheingold, A. L., Hecht, D. A. & Gustafson, J. L. (2015). *Angew. Chem. Int. Ed.* **54**, 11754–11759.
Spackman, M. A. & Jayatilaka, D. (2009). *CrystEngComm*, **11**, 19–32.
Tinsley, R. A. & Walter, N. G. (2006). *RNA*, **12**, 522–529.
Toenjes, S. T. & Gustafson, J. L. (2018). *Future Med. Chem.* **10**, 409–422.
Tokugawa, M., Masaki, Y., Canggadibrata, J. C., Kaneko, K., Shiozawa, T., Kanamori, T., Grøtli, M., Wilhelmsson, L. M., Sekine, M. & Seio, K. (2016). *Chem. Commun.* **52**, 3809–3812.
Turner, M. J., McKinnon, J. J., Wolff, S. K., Grimwood, D. J., Spackman, P. R., Jayatilaka, D. & Spackman, M. A. (2017). *CrystalExplorer17*. University of Western Australia. http://hirshfeldsurface.net.
Van Wijk, L., Haasnoot, C. A. G., de Leeuw, F. A. A. M., Huckriede, B. D., Westra Hoekzema, A. J. A. & Altona, C. (1999). *PSEUROT 6.3*. Leiden Institute of Chemistry, Leiden University, The Netherlands.
Wahba, A. S., Esmaeili, A., Damha, M. J. & Hudson, R. H. E. (2010). *Nucleic Acids Res.* **38**, 1048–1056.
Wilhelmsson, L. M. (2010). *Q. Rev. Biophys.* **43**, 159–183.
Young, D. W. & Wilson, H. R. (1975). *Acta Cryst.* B**31**, 961–965.

supporting information

Acta Cryst. (2022). C**78**, 141-147 [https://doi.org/10.1107/S2053229622001000]

8-Furylimidazolo-2′-deoxycytidine: crystal structure, packing, atropisomerism and fluorescence

Simone Budow-Busse, Sunit K. Jana, Dasharath Kondhare, Constantin Daniliuc and Frank Seela

Computing details

Data collection: *APEX3* (Bruker, 2016); cell refinement: *SAINT* (Bruker, 2015); data reduction: *SAINT* (Bruker, 2015); program(s) used to solve structure: SHELXT2014 (Sheldrick, 2015a); program(s) used to refine structure: *SHELXL2018* (Sheldrick, 2015b); molecular graphics: shelXle (Hübschle *et al.*, 2011); software used to prepare material for publication: *SHELXL2014* (Sheldrick, 2015b).

8-Furylimidazolo-2′-deoxycytidine

Crystal data

$C_{14}H_{14}N_4O_5$
M_r = 318.29
Orthorhombic, $P2_12_12_1$
a = 5.3043 (4) Å
b = 11.1405 (8) Å
c = 22.6067 (18) Å
V = 1335.89 (18) Å^3
Z = 4
$F(000)$ = 664
D_x = 1.583 Mg m^{-3}
Cu $K\alpha$ radiation, λ = 1.54178 Å
Cell parameters from 9220 reflections
θ = 4.4–61.4°
μ = 1.04 mm^{-1}
T = 100 K
Needle, colourless
0.38 × 0.06 × 0.03 mm

Data collection

Bruker D8 Venture PHOTON 100 CMOS diffractometer
Radiation source: Cu ImS, micro focus tube
MX mirror monochromator
Detector resolution: 10.4167 pixels mm^{-1}
ω and phi scans
Absorption correction: multi-scan (SADABS; Bruker, 2014)
T_{min} = 0.69, T_{max} = 0.97
28381 measured reflections
2241 independent reflections
1559 reflections with $I > 2\sigma(I)$
R_{int} = 0.149
θ_{max} = 65.1°, θ_{min} = 4.4°
h = −6→6
k = −12→13
l = −26→26

Refinement

Refinement on F^2
Least-squares matrix: full
$R[F^2 > 2\sigma(F^2)]$ = 0.053
$wR(F^2)$ = 0.142
S = 1.03
2241 reflections
335 parameters
279 restraints
Primary atom site location: structure-invariant direct methods
Hydrogen site location: mixed
H atoms treated by a mixture of independent and constrained refinement
$w = 1/[\sigma^2(F_o^2) + (0.0671P)^2 + 0.4487P]$ where $P = (F_o^2 + 2F_c^2)/3$
$(\Delta/\sigma)_{max} < 0.001$

$\Delta\rho_{max}$ = 0.22 e Å^{-3}
$\Delta\rho_{min}$ = −0.20 e Å^{-3}

Absolute structure: Flack *x* determined using 503 quotients [(I+)-(I-)]/[(I+)+(I-)] (Parsons *et al.*, 2013)
Absolute structure parameter: 0.0 (3)

Special details

Geometry. All esds (except the esd in the dihedral angle between two l.s. planes) are estimated using the full covariance matrix. The cell esds are taken into account individually in the estimation of esds in distances, angles and torsion angles; correlations between esds in cell parameters are only used when they are defined by crystal symmetry. An approximate (isotropic) treatment of cell esds is used for estimating esds involving l.s. planes.

Refinement. Reflections were merged by SHELXL according to the crystal class for the calculation of statistics and refinement.
_reflns_Friedel_fraction is defined as the number of unique Friedel pairs measured divided by the number that would be possible theoretically, ignoring centric projections and systematic absences.
The furyl ring and the sugar moiety linked to nitrogen atom N1 are disordered over two positions. Several restraints (SADI, SAME, ISOR and SIMU) were used in order to improve refinement stability.
The hydrogen at N9 atom was refined freely, but with N-H distance restraints (DFIX).

Fractional atomic coordinates and isotropic or equivalent isotropic displacement parameters (Å^2)

	x	*y*	*z*	U_{iso}*/U_{eq}	Occ. (<1)
N3	0.1129 (9)	0.7536 (4)	0.4332 (2)	0.0469 (12)	
N9	0.4585 (9)	0.6261 (4)	0.4609 (2)	0.0477 (12)	
H9	0.507 (14)	0.649 (6)	0.4959 (18)	0.09 (3)*	
N7	0.4582 (9)	0.4957 (4)	0.3847 (2)	0.0481 (12)	
O2	−0.2073 (8)	0.8584 (4)	0.39022 (17)	0.0552 (11)	
C2	−0.0592 (11)	0.7718 (5)	0.3895 (3)	0.0477 (14)	
C4	0.2677 (11)	0.6617 (5)	0.4252 (2)	0.0455 (14)	
C5	0.2673 (11)	0.5813 (5)	0.3773 (2)	0.0457 (14)	
C6	0.0902 (11)	0.5990 (5)	0.3348 (3)	0.0486 (14)	
H6	0.079984	0.547501	0.301383	0.058*	
C8	0.5657 (11)	0.5260 (5)	0.4345 (3)	0.0471 (14)	
C2"	0.776 (3)	0.4681 (16)	0.4641 (7)	0.042 (4)	0.69 (2)
C3"	0.914 (4)	0.4913 (18)	0.5147 (8)	0.050 (4)	0.69 (2)
H3"	0.890201	0.554563	0.54235	0.06*	0.69 (2)
C4"	1.101 (3)	0.3981 (15)	0.5160 (7)	0.050 (4)	0.69 (2)
H4"	1.225476	0.388121	0.545744	0.06*	0.69 (2)
C5"	1.070 (4)	0.3263 (16)	0.4678 (8)	0.054 (4)	0.69 (2)
H5"	1.172166	0.259499	0.457466	0.065*	0.69 (2)
O1"	0.869 (2)	0.3668 (12)	0.4372 (6)	0.045 (3)	0.69 (2)
C2"A	0.775 (7)	0.455 (4)	0.4520 (15)	0.045 (9)	0.31 (2)
C3"A	0.909 (8)	0.360 (4)	0.4310 (19)	0.048 (10)	0.31 (2)
H3"A	0.892394	0.3163	0.39495	0.057*	0.31 (2)
C4"A	1.083 (7)	0.343 (3)	0.4792 (13)	0.033 (7)	0.31 (2)
H4"A	1.19976	0.278551	0.480687	0.04*	0.31 (2)
C5"A	1.068 (7)	0.427 (3)	0.5223 (14)	0.046 (8)	0.31 (2)
H5"A	1.168257	0.435096	0.556882	0.055*	0.31 (2)
O1"A	0.873 (5)	0.497 (3)	0.5041 (13)	0.057 (8)	0.31 (2)
N1	−0.0699 (9)	0.6911 (4)	0.3414 (2)	0.0479 (12)	
C1′	−0.2601 (19)	0.7147 (9)	0.2951 (4)	0.052 (3)	0.867 (10)

H1′	−0.40721	0.757227	0.313121	0.063*	0.867 (10)
C2′	−0.169 (3)	0.7849 (9)	0.2420 (5)	0.054 (3)	0.867 (10)
H2′1	0.007913	0.764452	0.232126	0.064*	0.867 (10)
H2′2	−0.181834	0.872482	0.248878	0.064*	0.867 (10)
C3′	−0.349 (2)	0.7439 (9)	0.1936 (4)	0.058 (3)	0.867 (10)
H3′	−0.270578	0.749845	0.153546	0.07*	0.867 (10)
O3′	−0.580 (2)	0.8086 (10)	0.1966 (7)	0.069 (4)	0.867 (10)
H3′1	−0.58981	0.855293	0.167492	0.103*	0.867 (10)
C4′	−0.401 (2)	0.6130 (8)	0.2109 (4)	0.054 (2)	0.867 (10)
H4′	−0.585565	0.596997	0.205767	0.064*	0.867 (10)
O4′	−0.3413 (17)	0.6022 (7)	0.2724 (3)	0.054 (2)	0.867 (10)
C5′	−0.258 (3)	0.5215 (9)	0.1764 (4)	0.061 (2)	0.867 (10)
H5′1	−0.275227	0.44217	0.195759	0.073*	0.867 (10)
H5′2	−0.329703	0.515396	0.136104	0.073*	0.867 (10)
O5′	−0.0023 (9)	0.5524 (5)	0.1728 (3)	0.070 (2)	0.867 (10)
H5′	0.074431	0.50092	0.152473	0.104*	0.867 (10)
C1′A	−0.265 (11)	0.712 (5)	0.297 (2)	0.055 (15)	0.133 (10)
H1′A	−0.427674	0.738532	0.314696	0.066*	0.133 (10)
C2′A	−0.168 (16)	0.802 (5)	0.251 (3)	0.042 (13)	0.133 (10)
H2′3	0.013982	0.790791	0.24334	0.05*	0.133 (10)
H2′4	−0.199933	0.88556	0.26376	0.05*	0.133 (10)
C3′A	−0.329 (13)	0.767 (4)	0.198 (2)	0.052 (14)	0.133 (10)
H3′A	−0.237828	0.782496	0.160268	0.062*	0.133 (10)
O3′A	−0.560 (15)	0.832 (6)	0.201 (4)	0.040 (14)	0.133 (10)
H3′2	−0.55881	0.886368	0.175222	0.06*	0.133 (10)
C4′A	−0.378 (14)	0.633 (4)	0.206 (2)	0.060 (15)	0.133 (10)
H4′A	−0.565743	0.62256	0.206731	0.072*	0.133 (10)
O4′A	−0.292 (13)	0.602 (4)	0.265 (2)	0.057 (13)	0.133 (10)
C5′A	−0.28 (2)	0.544 (4)	0.164 (2)	0.074 (15)	0.133 (10)
H5′3	−0.37983	0.547777	0.12687	0.088*	0.133 (10)
H5′4	−0.103079	0.56497	0.15359	0.088*	0.133 (10)
O5′A	−0.284 (8)	0.423 (3)	0.1853 (15)	0.073 (13)	0.133 (10)
H5′A	−0.400708	0.416009	0.2102	0.109*	0.133 (10)

Atomic displacement parameters (Å²)

	U^{11}	U^{22}	U^{33}	U^{12}	U^{13}	U^{23}
N3	0.042 (3)	0.045 (3)	0.054 (3)	0.001 (2)	0.001 (2)	0.001 (2)
N9	0.042 (3)	0.048 (3)	0.053 (3)	−0.002 (3)	0.003 (3)	−0.002 (3)
N7	0.043 (3)	0.043 (3)	0.059 (3)	0.000 (2)	0.004 (3)	−0.004 (2)
O2	0.050 (2)	0.050 (2)	0.066 (3)	0.007 (2)	0.002 (2)	0.000 (2)
C2	0.044 (3)	0.043 (3)	0.056 (4)	−0.004 (3)	0.009 (3)	0.002 (3)
C4	0.035 (3)	0.048 (3)	0.053 (3)	−0.005 (3)	0.003 (3)	0.004 (3)
C5	0.040 (3)	0.044 (3)	0.054 (4)	−0.007 (3)	0.005 (3)	−0.003 (3)
C6	0.041 (3)	0.048 (4)	0.057 (4)	−0.003 (3)	0.005 (3)	−0.003 (3)
C8	0.039 (3)	0.045 (3)	0.057 (3)	−0.004 (3)	0.009 (3)	0.000 (3)
C2"	0.039 (5)	0.041 (5)	0.045 (6)	0.002 (4)	0.005 (5)	−0.006 (5)
C3"	0.050 (7)	0.050 (6)	0.049 (6)	−0.010 (5)	−0.002 (5)	0.002 (5)

C4"	0.038 (5)	0.051 (6)	0.060 (6)	0.006 (5)	0.001 (4)	−0.001 (5)
C5"	0.047 (6)	0.058 (6)	0.058 (7)	−0.001 (5)	−0.001 (5)	−0.005 (5)
O1"	0.030 (5)	0.048 (5)	0.059 (5)	0.003 (3)	0.003 (4)	−0.007 (3)
C2"A	0.041 (11)	0.046 (11)	0.048 (11)	−0.007 (7)	0.004 (6)	0.001 (7)
C3"A	0.045 (12)	0.046 (11)	0.053 (11)	0.002 (7)	0.003 (7)	−0.004 (6)
C4"A	0.027 (8)	0.038 (9)	0.035 (9)	0.007 (6)	−0.001 (6)	−0.004 (6)
C5"A	0.044 (10)	0.043 (10)	0.052 (9)	−0.009 (7)	0.006 (6)	−0.004 (6)
O1"A	0.056 (10)	0.055 (9)	0.059 (10)	0.005 (6)	−0.001 (6)	0.001 (6)
N1	0.042 (3)	0.048 (3)	0.053 (3)	−0.001 (2)	0.002 (2)	0.000 (2)
C1′	0.042 (4)	0.051 (4)	0.064 (4)	−0.005 (3)	−0.003 (3)	0.000 (3)
C2′	0.046 (4)	0.050 (5)	0.065 (5)	0.005 (4)	0.004 (4)	0.004 (4)
C3′	0.049 (4)	0.059 (5)	0.067 (4)	0.000 (4)	0.004 (3)	0.008 (4)
O3′	0.040 (4)	0.070 (6)	0.097 (7)	0.010 (5)	0.004 (4)	0.027 (5)
C4′	0.048 (4)	0.055 (4)	0.057 (4)	−0.003 (4)	−0.001 (3)	0.005 (3)
O4′	0.052 (4)	0.053 (3)	0.057 (3)	−0.010 (3)	0.000 (3)	0.003 (3)
C5′	0.060 (5)	0.062 (5)	0.060 (4)	−0.004 (4)	−0.006 (4)	0.000 (4)
O5′	0.044 (3)	0.059 (4)	0.106 (5)	−0.006 (2)	0.006 (3)	−0.021 (3)
C1′A	0.053 (16)	0.055 (16)	0.058 (16)	−0.001 (7)	0.000 (7)	0.000 (7)
C2′A	0.040 (14)	0.042 (14)	0.043 (14)	0.001 (7)	0.000 (7)	−0.001 (7)
C3′A	0.052 (15)	0.051 (15)	0.053 (15)	0.001 (7)	0.002 (7)	0.003 (7)
O3′A	0.044 (18)	0.037 (17)	0.037 (17)	−0.004 (12)	−0.002 (12)	−0.012 (12)
C4′A	0.060 (16)	0.061 (16)	0.060 (16)	0.000 (7)	−0.001 (7)	0.000 (7)
O4′A	0.058 (15)	0.057 (14)	0.056 (14)	−0.003 (7)	0.000 (7)	0.000 (7)
C5′A	0.074 (16)	0.074 (16)	0.074 (16)	−0.002 (7)	0.000 (7)	0.001 (7)
O5′A	0.079 (17)	0.064 (17)	0.074 (16)	0.003 (12)	−0.005 (12)	−0.005 (12)

Geometric parameters (Å, º)

N3—C4	1.324 (7)	C1′—C2′	1.512 (9)
N3—C2	1.361 (7)	C1′—H1′	1.0
N9—C4	1.353 (7)	C2′—C3′	1.524 (10)
N9—C8	1.387 (7)	C2′—H2′1	0.99
N9—H9	0.87 (3)	C2′—H2′2	0.99
N7—C8	1.307 (7)	C3′—O3′	1.420 (9)
N7—C5	1.401 (7)	C3′—C4′	1.535 (11)
O2—C2	1.244 (6)	C3′—H3′	1.0
C2—N1	1.413 (7)	O3′—H3′1	0.84
C4—C5	1.406 (8)	C4′—O4′	1.432 (8)
C5—C6	1.358 (8)	C4′—C5′	1.491 (11)
C6—N1	1.340 (7)	C4′—H4′	1.0
C6—H6	0.95	C5′—O5′	1.403 (15)
C8—C2"A	1.418 (19)	C5′—H5′1	0.99
C8—C2"	1.451 (11)	C5′—H5′2	0.99
C2"—O1"	1.374 (15)	O5′—H5′	0.84
C2"—C3"	1.38 (2)	C1′A—O4′A	1.43 (3)
C3"—C4"	1.44 (2)	C1′A—C2′A	1.52 (3)
C3"—H3"	0.95	C1′A—H1′A	1.0
C4"—C5"	1.363 (14)	C2′A—C3′A	1.52 (3)

C4"—H4"	0.95	C2′A—H2′3	0.99
C5"—O1"	1.348 (16)	C2′A—H2′4	0.99
C5"—H5"	0.95	C3′A—O3′A	1.43 (3)
C2"A—C3"A	1.37 (3)	C3′A—C4′A	1.53 (3)
C2"A—O1"A	1.37 (3)	C3′A—H3′A	1.0
C3"A—C4"A	1.44 (3)	O3′A—H3′2	0.84
C3"A—H3"A	0.95	C4′A—O4′A	1.44 (3)
C4"A—C5"A	1.35 (2)	C4′A—C5′A	1.48 (3)
C4"A—H4"A	0.95	C4′A—H4′A	1.0
C5"A—O1"A	1.36 (3)	C5′A—O5′A	1.43 (3)
C5"A—H5"A	0.95	C5′A—H5′3	0.99
N1—C1′A	1.47 (3)	C5′A—H5′4	0.99
N1—C1′	1.477 (8)	O5′A—H5′A	0.84
C1′—O4′	1.420 (8)		

C4—N3—C2	115.6 (5)	C1′—C2′—H2′1	111.3
C4—N9—C8	106.7 (5)	C3′—C2′—H2′1	111.3
C4—N9—H9	133 (5)	C1′—C2′—H2′2	111.3
C8—N9—H9	120 (5)	C3′—C2′—H2′2	111.3
C8—N7—C5	104.0 (5)	H2′1—C2′—H2′2	109.2
O2—C2—N3	122.0 (5)	O3′—C3′—C2′	110.8 (8)
O2—C2—N1	118.6 (5)	O3′—C3′—C4′	108.4 (8)
N3—C2—N1	119.4 (5)	C2′—C3′—C4′	102.4 (6)
N3—C4—N9	127.5 (5)	O3′—C3′—H3′	111.6
N3—C4—C5	126.6 (6)	C2′—C3′—H3′	111.6
N9—C4—C5	105.8 (5)	C4′—C3′—H3′	111.6
C6—C5—N7	133.1 (5)	C3′—O3′—H3′1	109.5
C6—C5—C4	117.0 (6)	O4′—C4′—C5′	109.7 (7)
N7—C5—C4	109.9 (5)	O4′—C4′—C3′	106.6 (6)
N1—C6—C5	118.1 (5)	C5′—C4′—C3′	115.2 (8)
N1—C6—H6	121.0	O4′—C4′—H4′	108.4
C5—C6—H6	121.0	C5′—C4′—H4′	108.4
N7—C8—N9	113.5 (5)	C3′—C4′—H4′	108.4
N7—C8—C2"A	116.1 (14)	C1′—O4′—C4′	110.1 (6)
N9—C8—C2"A	130.4 (14)	O5′—C5′—C4′	110.8 (8)
N7—C8—C2"	128.2 (8)	O5′—C5′—H5′1	109.5
N9—C8—C2"	118.3 (8)	C4′—C5′—H5′1	109.5
O1"—C2"—C3"	109.2 (9)	O5′—C5′—H5′2	109.5
O1"—C2"—C8	115.9 (12)	C4′—C5′—H5′2	109.5
C3"—C2"—C8	134.9 (14)	H5′1—C5′—H5′2	108.1
C2"—C3"—C4"	104.3 (15)	C5′—O5′—H5′	109.5
C2"—C3"—H3"	127.8	O4′A—C1′A—N1	106 (3)
C4"—C3"—H3"	127.8	O4′A—C1′A—C2′A	105 (3)
C5"—C4"—C3"	109.0 (14)	N1—C1′A—C2′A	109 (4)
C5"—C4"—H4"	125.5	O4′A—C1′A—H1′A	111.9
C3"—C4"—H4"	125.5	N1—C1′A—H1′A	111.9
O1"—C5"—C4"	108.0 (14)	C2′A—C1′A—H1′A	111.9
O1"—C5"—H5"	126.0	C1′A—C2′A—C3′A	100 (2)

C4"—C5"—H5"	126.0	C1′A—C2′A—H2′3	111.8
C5"—O1"—C2"	109.4 (12)	C3′A—C2′A—H2′3	111.8
C3"A—C2"A—O1"A	111.7 (18)	C1′A—C2′A—H2′4	111.8
C3"A—C2"A—C8	138 (3)	C3′A—C2′A—H2′4	111.8
O1"A—C2"A—C8	110 (2)	H2′3—C2′A—H2′4	109.5
C2"A—C3"A—C4"A	100 (2)	O3′A—C3′A—C2′A	109 (3)
C2"A—C3"A—H3"A	130.2	O3′A—C3′A—C4′A	110 (4)
C4"A—C3"A—H3"A	130.2	C2′A—C3′A—C4′A	105 (2)
C5"A—C4"A—C3"A	115 (3)	O3′A—C3′A—H3′A	111.1
C5"A—C4"A—H4"A	122.6	C2′A—C3′A—H3′A	111.1
C3"A—C4"A—H4"A	122.6	C4′A—C3′A—H3′A	111.1
C4"A—C5"A—O1"A	103 (2)	C3′A—O3′A—H3′2	109.5
C4"A—C5"A—H5"A	128.5	O4′A—C4′A—C5′A	109 (3)
O1"A—C5"A—H5"A	128.5	O4′A—C4′A—C3′A	107 (2)
C5"A—O1"A—C2"A	111 (2)	C5′A—C4′A—C3′A	121 (4)
C6—N1—C2	123.2 (5)	O4′A—C4′A—H4′A	106.4
C6—N1—C1′A	119 (2)	C5′A—C4′A—H4′A	106.4
C2—N1—C1′A	117 (2)	C3′A—C4′A—H4′A	106.4
C6—N1—C1′	119.4 (6)	C1′A—O4′A—C4′A	107 (2)
C2—N1—C1′	117.4 (6)	O5′A—C5′A—C4′A	114 (4)
O4′—C1′—N1	107.8 (6)	O5′A—C5′A—H5′3	108.9
O4′—C1′—C2′	105.5 (6)	C4′A—C5′A—H5′3	108.9
N1—C1′—C2′	115.8 (7)	O5′A—C5′A—H5′4	108.9
O4′—C1′—H1′	109.2	C4′A—C5′A—H5′4	108.9
N1—C1′—H1′	109.2	H5′3—C5′A—H5′4	107.7
C2′—C1′—H1′	109.2	C5′A—O5′A—H5′A	109.5
C1′—C2′—C3′	102.3 (6)		

C4—N3—C2—O2	−176.5 (5)	C5—C6—N1—C1′	178.3 (7)
C4—N3—C2—N1	2.9 (7)	O2—C2—N1—C6	176.2 (5)
C2—N3—C4—N9	178.2 (5)	N3—C2—N1—C6	−3.2 (8)
C2—N3—C4—C5	−1.4 (8)	O2—C2—N1—C1′A	−3 (3)
C8—N9—C4—N3	179.7 (5)	N3—C2—N1—C1′A	178 (3)
C8—N9—C4—C5	−0.6 (6)	O2—C2—N1—C1′	−0.6 (9)
C8—N7—C5—C6	−179.8 (6)	N3—C2—N1—C1′	180.0 (6)
C8—N7—C5—C4	−0.5 (6)	C6—N1—C1′—O4′	35.8 (10)
N3—C4—C5—C6	−0.2 (8)	C2—N1—C1′—O4′	−147.2 (7)
N9—C4—C5—C6	−179.9 (5)	C6—N1—C1′—C2′	−82.1 (10)
N3—C4—C5—N7	−179.6 (5)	C2—N1—C1′—C2′	94.9 (8)
N9—C4—C5—N7	0.7 (6)	O4′—C1′—C2′—C3′	35.0 (10)
N7—C5—C6—N1	179.4 (6)	N1—C1′—C2′—C3′	154.2 (8)
C4—C5—C6—N1	0.2 (8)	C1′—C2′—C3′—O3′	82.1 (10)
C5—N7—C8—N9	0.1 (6)	C1′—C2′—C3′—C4′	−33.3 (9)
C5—N7—C8—C2"A	−178 (2)	O3′—C3′—C4′—O4′	−96.2 (11)
C5—N7—C8—C2"	179.8 (12)	C2′—C3′—C4′—O4′	21.0 (10)
C4—N9—C8—N7	0.3 (7)	O3′—C3′—C4′—C5′	141.8 (10)
C4—N9—C8—C2"A	178 (3)	C2′—C3′—C4′—C5′	−101.0 (10)
C4—N9—C8—C2"	−179.4 (10)	N1—C1′—O4′—C4′	−147.0 (8)

N7—C8—C2"—O1"	−2 (2)	C2′—C1′—O4′—C4′	−22.7 (10)
N9—C8—C2"—O1"	177.7 (12)	C5′—C4′—O4′—C1′	126.1 (10)
N7—C8—C2"—C3"	177.1 (19)	C3′—C4′—O4′—C1′	0.8 (11)
N9—C8—C2"—C3"	−3 (3)	O4′—C4′—C5′—O5′	−73.0 (10)
O1"—C2"—C3"—C4"	1 (2)	C3′—C4′—C5′—O5′	47.3 (10)
C8—C2"—C3"—C4"	−178 (2)	C6—N1—C1′A—O4′A	19 (5)
C2"—C3"—C4"—C5"	1 (2)	C2—N1—C1′A—O4′A	−162 (3)
C3"—C4"—C5"—O1"	−2 (2)	C6—N1—C1′A—C2′A	−94 (4)
C4"—C5"—O1"—C2"	3 (2)	C2—N1—C1′A—C2′A	86 (4)
C3"—C2"—O1"—C5"	−2 (2)	O4′A—C1′A—C2′A—C3′A	41 (5)
C8—C2"—O1"—C5"	177.0 (16)	N1—C1′A—C2′A—C3′A	155 (4)
N7—C8—C2"A—C3"A	1 (7)	C1′A—C2′A—C3′A—O3′A	88 (6)
N9—C8—C2"A—C3"A	−177 (5)	C1′A—C2′A—C3′A—C4′A	−30 (5)
N7—C8—C2"A—O1"A	179 (3)	O3′A—C3′A—C4′A—O4′A	−107 (6)
N9—C8—C2"A—O1"A	1 (5)	C2′A—C3′A—C4′A—O4′A	10 (6)
O1"A—C2"A—C3"A—C4"A	5 (6)	O3′A—C3′A—C4′A—C5′A	128 (6)
C8—C2"A—C3"A—C4"A	−177 (5)	C2′A—C3′A—C4′A—C5′A	−115 (7)
C2"A—C3"A—C4"A—C5"A	−5 (6)	N1—C1′A—O4′A—C4′A	−152 (5)
C3"A—C4"A—C5"A—O1"A	3 (5)	C2′A—C1′A—O4′A—C4′A	−37 (6)
C4"A—C5"A—O1"A—C2"A	0 (5)	C5′A—C4′A—O4′A—C1′A	149 (6)
C3"A—C2"A—O1"A—C5"A	−4 (6)	C3′A—C4′A—O4′A—C1′A	16 (6)
C8—C2"A—O1"A—C5"A	178 (3)	O4′A—C4′A—C5′A—O5′A	40 (8)
C5—C6—N1—C2	1.5 (8)	C3′A—C4′A—C5′A—O5′A	164 (6)
C5—C6—N1—C1′A	−179 (3)		

Hydrogen-bond geometry (Å, º)

D—H···*A*	*D*—H	H···*A*	*D*···*A*	*D*—H···*A*
N9—H9···N3^{i}	0.87 (3)	2.01 (3)	2.863 (7)	165 (6)
O3′a—H3′1a···N7^{ii}	0.84	2.08	2.852 (16)	153
C4′a—H4′a···O5′a^{iii}	1.0	2.39	3.370 (12)	168
O5′a—H5′a···O2^{iv}	0.84	1.99	2.818 (6)	169

Symmetry codes: (i) *x*+1/2, −*y*+3/2, −*z*+1; (ii) −*x*, *y*+1/2, −*z*+1/2; (iii) *x*−1, *y*, *z*; (iv) −*x*, *y*−1/2, −*z*+1/2.